Stopping a reaction-diffusion front

Jean-Guy Caputo [1,*], Gustavo Cruz-Pacheco,[2] and Benoît Sarels [3]

[1]*Laboratoire de Mathématiques, INSA Rouen Normandie - B.P. 8, Avenue de l'Université, 76801 Saint-Etienne du Rouvray, France*
[2]*Departmento Matemáticas y Mecánica, I.I.M.A.S.-U.N.A.M., Apdo. Postal 20–726, 01000 México D.F., México*
[3]*Sorbonne Université, CNRS, Université de Paris, Laboratoire Jacques-Louis Lions (LJLL), F-75005 Paris, France*

We revisit the problem of pinning a reaction-diffusion front by a defect, in particular by a reaction-free region. Using collective variables for the front and numerical simulations, we compare the behaviors of a bistable and monostable front. A bistable front can be pinned as confirmed by a pinning criterion, the analysis of the time independent problem, and simulations. Conversely, a monostable front can never be pinned, it gives rise to a secondary pulse past the defect and we calculate the time this pulse takes to appear. These radically different behaviors of bistable and monostable fronts raise issues for modelers in particular areas of biology, as for example, the study of tumor growth in the presence of different tissues.

I. INTRODUCTION

Reaction-diffusion equations are general models for active chemical reactions like combustion [1], see the book by Scott [2] for examples, or the review [3]. In biology, while these equations are ubiquitous in population dynamics or population genetics, they are also used in a variety of problems such as nerve impulse propagation in an axon or growth of a cancer tumor [4], see the general book by Murray [5]. These equations have a number of stationary solutions. In the physics context, the models have three stationary solutions, two stable and one unstable, they are termed *bistable*. In biology, the bistable model can be used to describe the growth of a population. Still, the main model remains the one that describes the wave of advance of an advantageous gene like in the seminal paper [6]. It only has two stationary states, one stable and another unstable; it is called *monostable*. The normal forms of these two different reaction terms are cubic for the bistable and quadratic for the monostable. Mostly the study of these two nonlinearities gives the qualitative picture for almost all other nonlinearities.

Important dynamical solutions are the fronts [in one dimension (1D)] that connect two such stationary solutions. In two dimensions (2D) and three dimensions (3D), assuming radial symmetry, fronts describe the interface of "blobs" where the inside has one state and the outside another. Fronts have a speed that is proportional to the square root of the diffusion times the reaction rate. Many studies dealt with the stability of such fronts, see [2] for references. Assuming a front is stable, important parameters are its position and width, i.e., the spatial extension of the transition region separating the two stationary states. These fronts have exact forms for the bistable [2] and monostable [7] nonlinearities. Using these solutions as Rayleigh-Ritz type ansatzes, we and other

authors have derived ordinary differential equations giving the evolution of the position and width—termed collective coordinates—whose solutions match remarkably well the full dynamics, see [8,9] for the bistable case and [10] for the monostable case.

For many applications it is useful to understand how fronts respond to perturbations of the environment. Such perturbations can be temporal such as the action of therapy on a cancer cell [11]. They can also be spatial like a defect in a burning candle. Such a geographic defect can act on scales larger or smaller than the front width. In the latter case, the front adiabatically adapts to the defect and changes its width and speed accordingly, see for example our study [8] on bistable fronts. When the defect is narrow compared to the front, a bistable front can be pinned by the defect [8]. This effect can also be seen in waveguides whose transverse width abruptly changes, see the works [12,13].

In this article we revisit the issue of front pinning comparing bistable and monostable fronts. We consider first as defect a region where the reaction is enhanced or diminished, but always remains strictly positive. We derive collective variable approximations for both fronts. A first result is that wide defects cannot pin any of the two types of fronts. Narrow defects will pin a bistable front, see the numerics and analysis of [8]. To understand further the phenomenon, we consider as defect a no reaction region of a given extension. Using collective variables for the front, we obtain a pinning criterion which indicates that static bistable fronts exist in such a region if it is large enough. This criterion is in excellent agreement with the solutions of the time-independent problem and the partial differential equation. Monostable fronts behave very differently, they can never be pinned. Numerical simulations show that a monostable front can be delayed and gives rise to a secondary pulse past the defect which will develop into a front that will continue to propagate. We calculated the delay time, i.e., the difference between the arrival at the defect and the appearance of the secondary pulse, when its maximum

*caputo@insa-rouen.fr

reaches 0.5. This delay time scales approximately linearly with the extension of the reaction-free region, in agreement with a simple calculation based on the diffusion kernel and the instability rate of the zero stationary solution.

The article is organized as follows. The bistable and monostable models and their exact solutions are recalled in Sec. II. Section III presents and discusses the collective variable differential equations for the front position and width. Sections IV and V detail the front motion in a no reaction zone for the bistable and monostable models, respectively. Section VI concludes the article.

II. THE MODEL

In the following we are concerned with the equation

$$u_t = u_{xx} + s(x)R(u),$$
$$u(x, 0) = u_0(x) \qquad (1)$$

for $(x, t) \in \mathbb{R} \times \mathbb{R}_+^*$ and u_0 a given function with sufficient regularity. We will study the two canonical types of nonlinearities: the monostable one $R(u) = u(1 - u)$ and the bistable one $R(u) = u(1 - u)(u - a)$ for some $0 < a < 1$. To account for the variable growth rate of the quantity u (chemical density, population density, etc.), we make use of a reactivity s that is space dependent and remains positive over the considered range: $s(x) > 0$ for every real x. Let us first recall the theory when s is constant. We recall that in the former case, the state $u^* = 1$ is a stable equilibrium of the associated ordinary differential equation while $u^* = 0$ is an unstable equilibrium. In the latter, the states $u^* = 0, 1$ are stable equilibria while $u^* = a$ is unstable.

To carry out our analysis in the next sections, we will use extensively the fact that exact solutions of Eq. (1) are known when s is constant. In the bistable case, all traveling wave solutions are fronts connecting the two stable equilibria. We choose to consider in the rest of the paper only fronts going from 1 at $-\infty$ to 0 at $+\infty$. Then all traveling wave solutions—up to a translation—are of the form

$$u(x, t) = \tilde{U}_{\text{bi}}(x - ct) = \frac{1}{1 + \exp\left[\sqrt{\frac{s}{2}}(x - ct)\right]}, \qquad (2)$$

where the speed c is known [2] and related to the parameter a via the formula

$$c = \sqrt{\frac{s}{2}}(1 - 2a). \qquad (3)$$

To consider only positive speeds, we will restrain—without loss of generality—our analysis to the range $0 < a < \frac{1}{2}$. In this case, the propagation of the front translates as an invasion of the state 0 by the state 1.

At each time the front is centered around $x = ct$, this means $u(ct, t) = \tilde{U}_{bi}(0) = \frac{1}{2}$. We can then define the width w of a given front by the relation

$$\tilde{U}_{\text{bi}}(-w) = \frac{1}{1 + e^{-1}} \approx 0.73$$

or equivalently $\tilde{U}_{\text{bi}}(w) = \frac{1}{1+e} \approx 0.27$. With that definition we have here

$$w = \sqrt{\frac{2}{s}}. \qquad (4)$$

In the monostable case, the situation is somewhat different. There are traveling wave solutions for a continuum of speeds $c \geqslant 2\sqrt{s}$, and here again traveling wave solutions are fronts going from 1 at $-\infty$ to 0 at $+\infty$. It is known that asymptotically a great number of solutions converge to the front of minimal speed $c = 2\sqrt{s}$. That is notably the case when u_0 is compactly supported [14]. Only one family of exact solutions is known [7], they take the form

$$u(x, t) = \tilde{U}_{\text{mono}}(x - ct) = \frac{1}{\left\{1 + K \exp\left[\sqrt{\frac{s}{6}}(x - ct)\right]\right\}^2}, \qquad (5)$$

where K is a constant and the speed is given by

$$c = 5\sqrt{\frac{s}{6}}. \qquad (6)$$

We will use this solution with $K = \sqrt{2} - 1$ to ensure that $\tilde{U}_{\text{mono}}(0) = \frac{1}{2}$. Here we define the width w of a given front by the relation

$$\tilde{U}_{\text{mono}}(-w) = \frac{1}{[1 + (\sqrt{2} - 1)e^{-1}]^2} \approx 0.75$$

or equivalently $\tilde{U}_{\text{mono}}(w) = \frac{1}{[1+(\sqrt{2}-1)e]^2} \approx 0.22$. With that definition we have

$$w = \sqrt{\frac{6}{s}}. \qquad (7)$$

Some differences between the bistable case and the monostable one are better understood when we see waves in the bistable case as being pushed by the bulk of the population distribution and waves in the monostable case wave as being pulled by the leading edge of the distribution [15].

III. COLLECTIVE VARIABLES

In the model we are interested in, the reactivity s is allowed to be space dependent. When the variations of s are small, it is reasonable to expect that the solutions of (1) will remain close to the solutions in the homogeneous case. This approach is sometimes called the use of collective variables. First, we can expect that the front remains close to its original profile but will move with a modulation of its speed:

$$u(x, t) \approx \tilde{U}[x - c(t)t].$$

Actually, the numerical simulations indicate that the solution behavior is better captured through a modulation of its center x_0 and width w:

$$u(x, t) \approx \tilde{U}\left(\frac{x - x_0(t)}{w(t)}\right).$$

When investigating the evolution of a compactly supported initial condition, for instance growing from near 0 values, it can also be useful to allow for a modulation of the amplitude

in the form of the following ansatz:

$$u(x, t) \approx A(t)\tilde{U}\left(\frac{x - x_0(t)}{w(t)}\right).$$

This kind of approach is used for instance in [10], where evolution equations for the collective variables are obtained through balance laws, just like in [8]. As our goal is to investigate the dynamics of established fronts, and not the evolution from an initial condition to a generalized traveling front, we will make no use here of this third collective variable.

That being said, in the context of this paper we will assume that at order zero we have

$$u(x, t) = U[x, x_0(t), w(t)] := (\tilde{U} \circ z)[x, x_0(t), w(t)], \quad (8)$$

where $\tilde{U}$ is a given profile and we define $z[x, x_0(t), w(t)] = \frac{x - x_0(t)}{w(t)}$. We can compute the time derivative and the second order space derivative

$$u_t = \dot{x}_0 \frac{\partial U}{\partial x_0} + \dot{w} \frac{\partial U}{\partial w},$$

$$u_{xx} = \frac{\partial^2 U}{\partial x^2}.$$

The next step is to obtain time evolution equations for the collective variables x_0 and w. To that end we follow the procedure exposed in [8,9]. After the analysis is carried over (details of the computations are given in Appendix A), we obtain the system of ordinary differential equations:

$$\dot{x}_0 = \frac{\alpha_1}{w} + \alpha_2 w K_0(x_0, w, s, R) + \alpha_3 w K_1(x_0, w, s, R), \quad (9a)$$

$$\dot{w} = \frac{\alpha_4}{w} + \alpha_5 w K_0(x_0, w, s, R) + \alpha_6 w K_1(x_0, w, s, R), \quad (9b)$$

where the α_i are numbers and the integrals K_n are given by

$$K_n(x_0, w, s, R) = \int_{-\infty}^{\infty} z^n s(wz + x_0) R[\tilde{U}(z)]\tilde{U}'(z) \, dz. \quad (10)$$

The integrals K_n are the main driver of the front time evolution, as we will see in the next sections.

A. Time-evolution equations for the collective variables

In the case of a bistable reaction term $R = R_b$, we are always able to compute the integrals because there is unicity of the profile

$$\tilde{U}(z) = \frac{1}{1 + \exp(z)} \quad (11)$$

and Eqs. (9) reduce to

$$\dot{x}_0 = -6w K_0(x_0, w, s, R_b), \quad (12a)$$

$$\dot{w} = \frac{3}{2(\pi^2 - 6)w} - \frac{18}{\pi^2 - 6} w K_1(x_0, w, s, R_b). \quad (12b)$$

These equations were obtained by Dawes and Susanto [9].

In the case of a monostable reaction term $R = R_m$, we are able to explicitly compute the integrals only when the profile $\tilde{U}$ is known. This is especially the case if we consider the simplest following ansatz:

$$\tilde{U}(z) = \frac{1}{[1 + (\sqrt{2} - 1)\exp(z)]^2}, \quad (13)$$

which is an exact solution of (1) when s is constant. Then Eqs. (9) give a system similar to (12) though a bit more intricate:

$$\dot{x}_0 = \frac{\alpha_1}{w} + \alpha_2 w K_0(x_0, w, s, R_m) + \alpha_3 w K_1(x_0, w, s, R_m), \quad (14a)$$

$$\dot{w} = \frac{\alpha_4}{w} + \alpha_5 w K_0(x_0, w, s, R_m) + \alpha_6 w K_1(x_0, w, s, R_m), \quad (14b)$$

and the constants are (see Appendix B for the definitions of the I_k)

$$\alpha_1 = \frac{90I_1}{85 - 12\pi^2} \approx -0.026, \quad \alpha_2 = \frac{900I_2}{85 - 12\pi^2} \approx -5.0,$$

$$\alpha_3 = \frac{900I_1}{12\pi^2 - 85} \approx 0.26, \quad \alpha_4 = \frac{18}{12\pi^2 - 85} \approx 0.54,$$

$$\alpha_5 = \frac{900I_1}{12\pi^2 - 85} \approx 0.26, \quad \alpha_6 = \frac{180}{85 - 12\pi^2} \approx -5.4.$$

B. Defect wide compared to the front width

For a defect that varies on a scale longer than w, $s(x_0 + wz) \approx s(x_0)$, so that s goes out of the integral, allowing us to take the computation one step further. We obtain for the bistable case

$$\dot{x}_0 = \frac{1 - 2a}{2} w s(x_0),$$

$$\dot{w} = \frac{3}{2(\pi^2 - 6)w} - \frac{3}{4(\pi^2 - 6)} w s(x_0), \quad (15)$$

and for the monostable case

$$\left(\frac{12\pi^2 - 85}{90}\right)\dot{x}_0 = \frac{5 - 6\ln(1 + \sqrt{2})}{30w}$$

$$+ \frac{30\pi^2 - 220 + 9\ln(1 + \sqrt{2})}{270} w s(x_0),$$

$$\left(\frac{12\pi^2 - 85}{90}\right)\dot{w} = \frac{1}{5w} - \frac{1}{30} w s(x_0). \quad (16)$$

These equations justify the notion of a local speed and width of the front. When $s(x) = s$ is constant, we recover the speeds and widths of the kinks, respectively, (3), (6) and (4), (7) in the homogeneous situation.

For both the bistable and monostable cases, the right-hand side of the $\dot{x}_0$ equation is always positive so that no pinning of the front occurs for wide defects. The numerical solutions match well the predictions given by (15) and (16), see [8,9] for the bistable case and [10] for the monostable case.

C. Defect narrow compared to the front width

We now turn our attention to defects that are narrow in comparison to the width of the incident front. Namely, we consider here the case of a Heaviside function. The defect function $s(x)$ can be written

$$s(x) = s_0 + s_1 H(x). \quad (17)$$

The integrals $K_i(x_0, w, s, R)$ can be broken down into two parts:

$$K_i(x_0, w, s, R) = s_0 \int_{-\infty}^{+\infty} + s_1 \int_{\frac{-x_0}{w}}^{+\infty} .$$

We introduce the expressions

$$K_i^l(u, R) = \int_{-\infty}^{u} z^i R[\tilde{U}(z)]\tilde{U}'(z)\, dz, \qquad (18a)$$

$$K_i^r(u, R) = \int_{u}^{+\infty} z^i R[\tilde{U}(z)]\tilde{U}'(z)\, dz, \qquad (18b)$$

with the exponents l for left and r for right. Then $K_i(x_0, w, s, R)$ for the defect (17) can be written as

$$K_i(x_0, w, s, R) = s_0 K_i(x_0, w, 1, R) + s_1 K_i^r\left(\frac{-x_0}{w}, R\right). \quad (19)$$

Then the system (9) reads

$$\dot{x}_0 = \frac{\alpha_1}{w} + ws_0[\alpha_2 K_0(x_0, w, 1, R) + \alpha_3 K_1(x_0, w, 1, R)]$$

$$+ ws_1\left[\alpha_2 K_0^r\left(\frac{-x_0}{w}, R\right) + \alpha_3 K_1^r\left(\frac{-x_0}{w}, R\right)\right], \qquad (20a)$$

$$\dot{w} = \frac{\alpha_4}{w} + ws_0(\alpha_5 K_0(x_0, w, 1, R) + \alpha_6 K_1(x_0, w, 1, R))$$

$$+ ws_1\left[\alpha_5 K_0^r\left(\frac{-x_0}{w}, R\right) + \alpha_6 K_1^r\left(\frac{-x_0}{w}, R\right)\right]. \qquad (20b)$$

Up to here, everything is reaction agnostic. We can, as we did earlier in Sec. III A, compute the different terms in this system. It has been done before for the bistable case [9], and the constants for the monostable one are given here in Appendix B. We write them here for the sake of completeness, first in the bistable case:

$$\dot{x}_0 = \frac{1 - 2a}{2}ws_0 - 6ws_1 K_0^r\left(\frac{-x_0}{w}, R\right), \qquad (21a)$$

$$\dot{w} = \frac{3}{2(\pi^2 - 6)w} + \frac{3}{4(6 - \pi^2)}ws_0$$

$$+ \frac{18}{6 - \pi^2}ws_1 K_1^r\left(\frac{-x_0}{w}, R\right) \qquad (21b)$$

and second in the monostable case:

$$\dot{x}_0 = -\frac{0.026}{w} + 0.83ws_0$$

$$- 5ws_1 K_0^r\left(\frac{-x_0}{w}, R\right) + 0.26ws_1 K_1^r\left(\frac{-x_0}{w}, R\right) \qquad (22a)$$

$$\dot{w} = \frac{0.54}{w} - 0.09ws_0$$

$$+ 0.26ws_1 K_0^r\left(\frac{-x_0}{w}, R\right) - 5.4ws_1 K_1^r\left(\frac{-x_0}{w}, R\right). \qquad (22b)$$

To illustrate how well the collective variables match with the PDE solution we consider a Heaviside defect (9) such that

$$s(x) = 0.2, \quad x < 0, \quad s(x) = 0.1, \quad x > 0.$$

Figure 1 shows $x_0(t)$, $w(t)$, $w(x_0)$ from left to right for both the monostable PDE and Eqs. (22a)–(22b). The values x_0, w are obtained by fitting the PDE solution by the ansatz (13) just as was done for the bistable solution in [8]. One can see the good agreement between the two solutions.
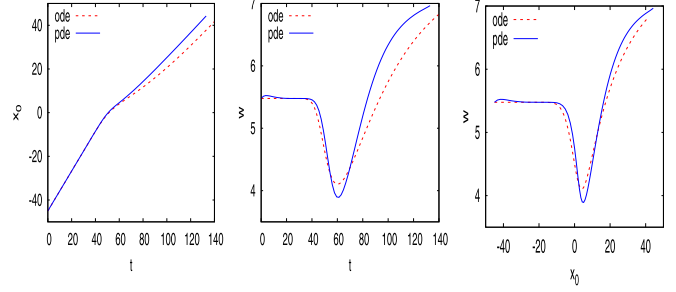

FIG. 1. Motion of a monostable front in a tanh-like defect $s = 0.2$, $x < 0$ and $s = 0.1$, $x > 0$. Both the PDE solutions in the continuous line (blue) and the reduced model in the dashed line (red) are presented. From left to right: $x_0(t)$, $w(t)$, $w(x_0)$.

D. Reaction-free region

Such a reaction-free zone occurs for example in forest fires where a trench with no trees is made to prevent fire propagation. In combustion in a duct, this corresponds to a region where there is no fuel. The defect function $s(x)$ can be written

$$s(x) = 0, \quad 0 \leqslant x \leqslant d, \quad s(x) = s_0 \quad \text{elsewhere.} \qquad (23)$$

With that defect, the integrals $K_i(x_0, w, s, R)$ break down into two parts:

$$K_i(x_0, w, s, R) = \int_{-\infty}^{\frac{-x_0}{w}} + \int_{\frac{d-x_0}{w}}^{+\infty},$$

with the naming conventions of (18). We get

$$K_i(x_0, w, s, R) = s_0 K_i^l\left(\frac{-x_0}{w}, R\right) + s_0 K_i^r\left(\frac{d - x_0}{w}, R\right) \qquad (24)$$

so that the system (9) reads

$$\dot{x}_0 = \frac{\alpha_1}{w} + ws_0\left[\alpha_2 K_0^l\left(\frac{-x_0}{w}, R\right) + \alpha_3 K_1^l\left(\frac{-x_0}{w}, R\right)\right]$$

$$+ ws_0\left[\alpha_2 K_0^r\left(\frac{d - x_0}{w}, R\right) + \alpha_3 K_1^r\left(\frac{d - x_0}{w}, R\right)\right], (25a)$$

$$\dot{w} = \frac{\alpha_4}{w} + ws_0\left[\alpha_5 K_0^l\left(\frac{-x_0}{w}, R\right) + \alpha_6 K_1^l\left(\frac{-x_0}{w}, R\right)\right]$$

$$+ ws_0\left[\alpha_5 K_0^r\left(\frac{d - x_0}{w}, R\right) + \alpha_6 K_1^r\left(\frac{d - x_0}{w}, R\right)\right]. (25b)$$

Again, up to here, the computation does not depend on the shape of the reaction term R.

IV. REACTION-FREE REGION FOR BISTABLE

In the bistable case, the major result is that the front can be stopped for a wide enough reaction-free zone. The analysis is developed in the following sections.

A. Criterion for front stopping

In this section, using the reduced model recalled above, we analyze the stopping of the front. For simplicity of the analysis we assume $s_0 = 1$ because the amplitude s_0 of the defect $s(x)$ can be scaled out of the problem by the following change of
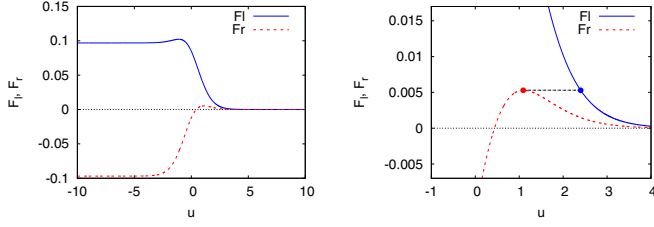
FIG. 2. Left: The functions $F^l(u, R_b)$ and $F^r(u, R_b)$. Right: Zoom on the $[-1, 4]$ region.

variables:

$$x = \frac{x'}{\sqrt{s_0}}, \quad t = \frac{t'}{s_0}, \quad s = s_0 s'(x'). \quad (26)$$

When the front stops x_0 and w are stationary. The collective variable ODEs (25) yield

$$-\frac{\alpha_1}{w} = w s_0 \Big[\alpha_2 K_0^l \Big(\frac{-x_0}{w}, R \Big) + \alpha_3 K_1^l \Big(\frac{-x_0}{w}, R \Big) \Big]$$
$$+ w s_0 \Big[\alpha_2 K_0^r \Big(\frac{d - x_0}{w}, R \Big) + \alpha_3 K_1^r \Big(\frac{d - x_0}{w}, R \Big) \Big], \quad (27a)$$

$$-\frac{\alpha_4}{w} = w s_0 \Big[\alpha_5 K_0^l \Big(\frac{-x_0}{w}, R \Big) + \alpha_6 K_1^l \Big(\frac{-x_0}{w}, R \Big) \Big]$$
$$+ w s_0 \Big[\alpha_5 K_0^r \Big(\frac{d - x_0}{w}, R \Big) + \alpha_6 K_1^r \Big(\frac{d - x_0}{w}, R \Big) \Big], \quad (27b)$$

then

$$-\frac{\alpha_1 \alpha_4}{w^2 s_0} = \alpha_2 \alpha_4 K_0^l \Big(\frac{-x_0}{w}, R \Big) + \alpha_3 \alpha_4 K_1^l \Big(\frac{-x_0}{w}, R \Big)$$
$$+ \alpha_2 \alpha_4 K_0^r \Big(\frac{d - x_0}{w}, R \Big) + \alpha_3 \alpha_4 K_1^r \Big(\frac{d - x_0}{w}, R \Big), \quad (28a)$$

$$-\frac{\alpha_1 \alpha_4}{w^2 s_0} = \alpha_1 \alpha_5 K_0^l \Big(\frac{-x_0}{w}, R \Big) + \alpha_1 \alpha_6 K_1^l \Big(\frac{-x_0}{w}, R \Big)$$
$$+ \alpha_1 \alpha_5 K_0^r \Big(\frac{d - x_0}{w}, R \Big) + \alpha_1 \alpha_6 K_1^r \Big(\frac{d - x_0}{w}, R \Big). \quad (28b)$$

The system implies an equation that can be written as

$$F^l \Big(\frac{x_0}{w}, R \Big) = F^r \Big(\frac{d - x_0}{w}, R \Big). \quad (29)$$

Equation (29) is verified for a critical distance

$$d = d_c \quad (30)$$

such that the following trichotomy happens:

(i) if $d < d_c$, the front is slowed down but it eventually crosses the no-reaction zone;

(ii) if $d = d_c$, the front is pinned in an infinite time, it converges towards a stationary solution;

(iii) if $d > d_c$, the front is pinned in a finite time.

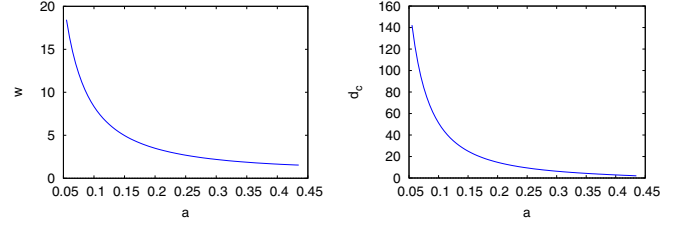FIG. 3. Left: Width of the front when pinning occurs as a function of the parameter a. Right: Critical distance of the reaction-free region as a function of the parameter a.

The feasibility of pinning can then easily be checked by studying the functions F^l and F^r; these are plotted in Fig. 2 for the bistable nonlinearity.

For the critical distance d_c, we need the maximum of F_r to cancel out the contribution from F_l. If we define $x_r = \text{Argmax}(F_r)$, $x_l = F_l^{-1}[\max(F_r)]$, then the following equations hold:

$$\frac{d_c - x_0}{w} = x_r, \quad (31a)$$

$$\frac{x_0}{w} = x_l. \quad (31b)$$

They give in turn w using (27b) (a bit of caution is necessary as $\alpha_1 = 0$ in the bistable case) and finally d_c. As an illustration, we plot in Fig. 3 the width of the front when pinning occurs (left panel), and the critical distance (right panel), as functions of the parameter a of the bistable reaction term. They compare very well with what we obtain through a simulation of the original PDE, as we will see in Fig. 6.

B. Stationary solution when the front stops

Let us consider the stationary case. The problem is

$$u_{xx} + u(1 - u)(u - a) = 0, \quad x \leqslant 0, \quad (32)$$

$$u_{xx} = 0, \quad 0 \leqslant x \leqslant d, \quad (33)$$

$$u_{xx} + u(1 - u)(u - a) = 0, \quad x \geqslant d, \quad (34)$$

together with the boundary conditions $u = 1$, $u_x = 0$, $x \to -\infty$ and $u = 0$, $u_x = 0$, $x \to \infty$. The interface conditions at $x = 0, d$ are continuity of u and of u_x. Multiplying (32) and (34) by u_x and integrating, we get

$$\frac{u_x^2}{2} + \Big(-\frac{u^4}{4} + \frac{u^3}{3}(a + 1) - \frac{u^2}{2}a \Big) = C_1, \quad x \leqslant 0,$$

$$\frac{u_x^2}{2} + \Big(-\frac{u^4}{4} + \frac{u^3}{3}(a + 1) - \frac{u^2}{2}a \Big) = 0, \quad x \geqslant d.$$

The constant C_1 is obtained from the first expression evaluated for $x \to -\infty$ where $u = 1$ and $u_x = 0$. We get

$$C_1 = \frac{1 - 2a}{12}. \quad (35)$$

Inside the strip $0 \leqslant x \leqslant d$, the solution is
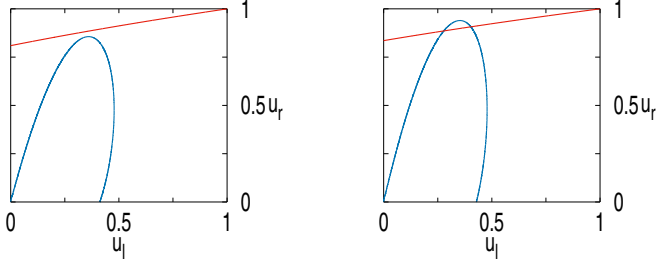
$$u = \alpha x + \beta.$$

FIG. 4. Bistable case, reaction-free region $0 \leqslant x \leqslant d$. Plots of the functions $g(u_l, u_r)$ (curve) and $h(u_l, u_r)$ (line) in the (u_l, u_r) plane for two different values of d, $d = 6 < d_c$ (left) and $d = 7 > d_c$ (right); the parameter is $a = 0.3$.

Using the interface conditions at $x = 0, d$, we get the two relations for the unknowns α, β:

$$\frac{\alpha^2}{2} - \frac{1}{4}\beta^4 + \frac{1}{3}(a + 1)\beta^3 - \frac{a}{2}\beta^2 = C_1, \qquad (36)$$

$$\frac{\alpha^2}{2} - \frac{1}{4}(\alpha d + \beta)^4 + \frac{1}{3}(a + 1)(\alpha d + \beta)^3$$
$$- \frac{a}{2}(\alpha d + \beta)^2 = 0. \qquad (37)$$

To solve this algebraic system we used a graphical method, introducing the values $u_l = \beta$ and $u_r = \alpha d + \beta$. In Fig. 4 we plot the 0 contour lines of the functions $g(u_l, u_r)$ and $h(u_l, u_r)$ defined by

$$g(u_l, u_r) = \frac{(u_l - u_r)^2}{2d^2} + f(u_l) - C_1, \qquad (38)$$

$$h(u_l, u_r) = \frac{(u_l - u_r)^2}{2d^2} + f(u_r), \qquad (39)$$

$$f(x) = -\frac{1}{4}x^4 + \frac{a + 1}{3}x^3 - \frac{a}{2}x^2, \qquad (40)$$

in the square $(u_l, u_r) \in [0, 1] \times [0, 1]$.

In the left panel $d < d_c$ so that there is no solution. In the right panel $d > d_c$ and there are two solutions (u_l, u_r). One of them is stable and the other unstable, as expected from standard bifurcation theory. A numerical exploration is then possible, e.g., by dichotomy, to find the value of d for which the line is tangent to the curve. This yields a second estimate for d_c after the one found in Sec. IV A.

C. Comparison of estimations of the critical widths d_c

We now have two means of estimating d_c, and will compare these estimates with the critical widths found by solving the original PDE.

Two typical PDE simulations are presented in Fig. 5 which shows snapshots of the solution $u(x, t)$ of (1) with $R(u) = u(1 - u)(u - 0.3)$ at different times, for $d = 6$ (left panel) and $d = 7$ (right panel). In the left panel, the front crosses the reaction-free region while it is pinned for the larger d shown in the right panel. Note that at the right edge of the defect, the value of u for a pinned front $(d > d_c)$ remains smaller than a. For the critical distance d_c, the stationary solution at the right edge of the front reaches a.
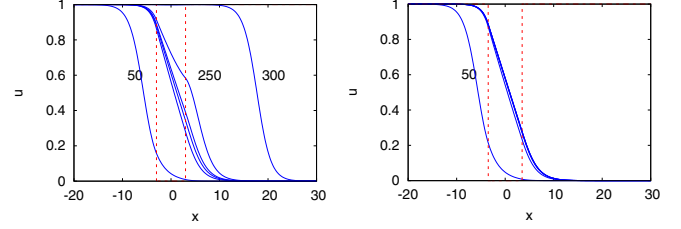

FIG. 5. Snapshots of u for $t = 50, 100, 150, 200, 250$, and 300 when the front crosses the reaction-free region $d = 6$ (left panel) and when the front is stopped by the reaction-free region $d = 7$ (right panel). The defect $s(x)$ is shown in the dashed line (red).

Using repeated simulations, we find a third approximate value of d_c. The estimates of d_c using the criterion, the analysis of the stationary solution and the PDE simulations are reported in Fig. 6. As seen, the estimates are in excellent agreement.

V. REACTION-FREE REGION FOR MONOSTABLE

A. Nonexistence of stationary solution

Following the same strategy as for the bistable case, we look for a stationary solution of the Fisher problem with a strip $[0, d]$. The formalism is the same as above. We then get

$$\frac{u_x^2}{2} + \left(\frac{u^2}{2} - \frac{u^3}{3}\right) = \frac{1}{6}, \quad x \leqslant 0.$$

$$\frac{u_x^2}{2} + \left(\frac{u^2}{2} - \frac{u^3}{3}\right) = 0, \quad x \geqslant d.$$

There is no solution to the problem because the second expression is always greater than 0, for $u \in [0, 1]$. This is consistent with the instability of the $u = 0$ stationary state for the monostable case.
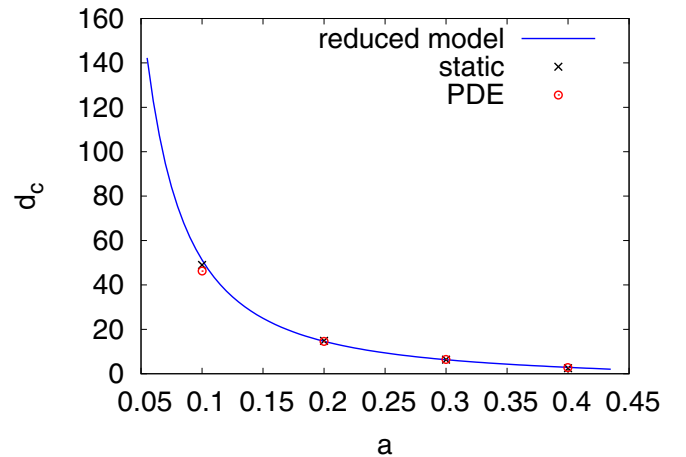

FIG. 6. Critical distance d_c of the reaction-free region for pinning to occur, as a function of the parameter a. The pinning criterion is shown together with estimates obtained using the stationary solution and the PDE solution.
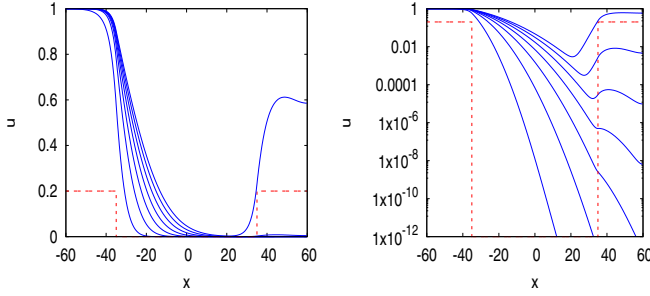
FIG. 7. Motion of a monostable front in a zero defect region of extension $d = 70$: snapshots of $u(x, t)$ for $t = 27.5, 55, 82.5, 110, 137.5, 165$, and 192.5 for a no reaction region of extension $d = 70$ in linear (left) and log (right) scales for u. The defect $s(x)$ is shown in the dashed line (red).

B. Appearance of secondary front

Figure 7 shows snapshots $u(x, t)$ of the solution for seven successive times from $t = 27.5$ up to 192.5 for a reaction-free region $|x| \leqslant 35$. The left panel shows the solution in linear scale. One can see the advancing profile for small u. It reaches the right interface and becomes visible at $t = 165$.

The increase of u with time is clearer in the right panel (log plot). There one sees the diffusion of u in the reaction-free zone followed by its amplification for $x \geqslant 35$.

The time of appearance of the secondary front can be estimated from the solution. Assume a reaction-free region

$$0 \leqslant x \leqslant d.$$

In Fig. 8 we plot the time interval $t_2 - t_1$ as a function of the half-width d of the reaction-free region. The instant t_1 corresponds to the front reaching the left edge of the strip, when its position is $x = 0$. The time t_2 is when the secondary pulse reaches the value 0.5.
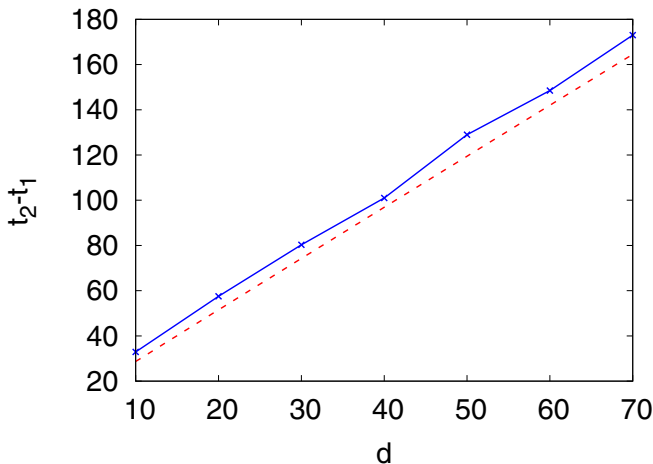

FIG. 8. Time of appearance of secondary front $t_2 - t_1$ for the monostable case for different widths of the reaction-free region. The continuous line (blue) corresponds to the numerical results and the dashed line (red) is for the approximation (44).

It is surprising that $t_2 - t_1$ depends linearly on d. To explain this effect, we suggest the following simple model. In the linear (no reaction) region, the propagation is governed by the heat kernel giving the solution at (x, t) for a source at $(y, t = 0)$,

$$K(x, y, t) = \frac{1}{\sqrt{4\pi t}} e^{-\frac{(x-y)^2}{4t}}. \tag{41}$$

Then for $x = d$, the solution of the heat equation u_h is $u_h(d, t) = \frac{1}{\sqrt{4\pi t}} e^{\frac{-d^2}{4t}}$. The $u = 0$ solution of the Fisher equation is unstable and any plane wave perturbation e^{ikx} will grow as

$$\delta u = e^{ikx + (s_0 - k^2)t}. \tag{42}$$

Combining (41) and (42), the solution of the Fisher equation at $x = d$ will be

$$u(d, t) = \frac{1}{\sqrt{4\pi t}} e^{-\frac{d^2}{4t} + s_0 t}, \tag{43}$$

where ξ is a coefficient smaller than 1 accounting for the average of the growth rate.

We can calculate when $u(d, t) = 0.5$. Using (43) we obtain

$$\frac{1}{\sqrt{4\pi t}} e^{-\frac{d^2}{4t} + s_0 t} = 0.5.$$

This implies

$$d = \sqrt{4 s_0 t^2 - 2t \log(\pi t)}. \tag{44}$$

In Fig. 8 we plotted the values of d, t such that $u(d, t) = 0.5$. These follow a straight dashed line (red) that is not far from to the numerical results (blue). During the time interval $t_2 - t_1$ a new pulse emerges right after the reaction-free region. After the instant t_2, this pulse gives rise to a front that travels towards the right at the same speed as before the defect. Comparing the front propagation with and without the defect shows that the front suffered a delay due to the defect.

VI. CONCLUSION

We analyzed the stopping of a one-dimensional reaction-diffusion front by a reaction-free region for bistable and monostable nonlinearities.

Bistable fronts can be stopped and—using a collective variable description—we obtained a stopping criterion linking the width of the region and the parameter of the nonlinearity. This criterion is in excellent agreement with the analysis of the time independent problem and the PDE solutions.

The monostable nonlinearity is more complex. If the front is accelerated by the defect, the collective variables agree well with the PDE numerical solution, otherwise a secondary pulse appears and the collective variable description is wrong. For a reaction-free region, a secondary pulse appears past the defect

and we can predict its time of appearance using a simple model based on the diffusion kernel and the growth rate of the zero unstable state.

This reaction-free region can be generalized into a damped-reaction region to model the action of (chemo/radio) therapy on a cancer tumor [11]. The function $s(x)$ becomes

$$s(x) = -s_1, \quad 0 \leqslant x \leqslant d, \quad s(x) = s_0 \quad \text{elsewhere.} \quad (45)$$

Using the same approach as for (43), we find the form of the solution in the damped-reaction region as

$$u(d, t) = \frac{1}{4\pi t} e^{\frac{d^2}{4t} + (s_0 - s_1)t}, \quad (46)$$

so that we can predict the time of crossing

$$d = \sqrt{4(s_0 - s_1)t^2 - 2t \log(\pi t)}. \quad (47)$$

The radically different behaviors between a monostable and a bistable front raise important questions for modelers. Is it reasonable that a monostable front cross a reaction-free region of arbitrary width? Maybe tumor researchers should use a $u^2(1-u)$ nonlinearity instead of the standard logistic. Then $u = 0$ would be stable and there would be a critical distance that the front could not cross.

ACKNOWLEDGMENT

APPENDIX A: DERIVATION OF THE TIME EVOLUTION EQUATIONS FOR THE COLLECTIVE VARIABLES

We multiply the equation

$$\dot{x}_0 \frac{\partial U}{\partial x_0} + \dot{w} \frac{\partial U}{\partial w} = \frac{\partial^2 U}{\partial x^2} + s(x)R\{U[x, x_0(t), w(t)]\}$$

by the test functions $\frac{\partial U}{\partial x_0}$ and $\frac{\partial U}{\partial w}$, respectively, and we integrate over x going from $-\infty$ to $+\infty$. We obtain

$$\dot{x}_0 \int_{-\infty}^{\infty} \left(\frac{\partial U}{\partial x_0}\right)^2 + \dot{w} \int_{-\infty}^{\infty} \frac{\partial U}{\partial x_0} \frac{\partial U}{\partial w}$$
$$= \int_{-\infty}^{\infty} \frac{\partial^2 U}{\partial x^2} \frac{\partial U}{\partial x_0} + \int_{-\infty}^{\infty} s(x)R\{U[x, x_0(t), w(t)]\} \frac{\partial U}{\partial x_0},$$
$$\dot{x}_0 \int_{-\infty}^{\infty} \frac{\partial U}{\partial x_0} \frac{\partial U}{\partial w} + \dot{w} \int_{-\infty}^{\infty} \left(\frac{\partial U}{\partial w}\right)^2$$
$$= \int_{-\infty}^{\infty} \frac{\partial^2 U}{\partial x^2} \frac{\partial U}{\partial w} + \int_{-\infty}^{\infty} s(x)R\{U[x, x_0(t), w(t)]\} \frac{\partial U}{\partial w}.$$

Thanks to the chain rule we have

$$\frac{\partial U}{\partial x} = \frac{1}{w} \tilde{U}'(z) \quad \text{and} \quad \frac{\partial^2 U}{\partial x^2} = \frac{1}{w^2} \tilde{U}''(z),$$
$$\frac{\partial U}{\partial x_0} = -\frac{1}{w} \tilde{U}'(z),$$
$$\frac{\partial U}{\partial w} = -\frac{z}{w} \tilde{U}'(z).$$

We remark that it is convenient to make the change of variable $z = \frac{x - x_0(t)}{w(t)}$ in each integral to get (after multiplication by w)

$$\dot{x}_0 \int_{-\infty}^{\infty} \tilde{U}'(z)^2 + \dot{w} \int_{-\infty}^{\infty} z\tilde{U}'(z)^2$$
$$= -\frac{1}{w} \int_{-\infty}^{\infty} \tilde{U}'(z)\tilde{U}''(z)$$
$$\quad - w \int_{-\infty}^{\infty} s(wz + x_0)R[\tilde{U}(z)]\tilde{U}'(z),$$
$$\dot{x}_0 \int_{-\infty}^{\infty} z\tilde{U}'(z)^2 + \dot{w} \int_{-\infty}^{\infty} z^2\tilde{U}'(z)^2$$
$$= -\frac{1}{w} \int_{-\infty}^{\infty} z\tilde{U}'(z)\tilde{U}''(z)$$
$$\quad - w \int_{-\infty}^{\infty} zs(wz + x_0)R[\tilde{U}(z)]\tilde{U}'(z).$$

The system is written in abstract form:

$$I_0 \dot{x}_0 + I_1 \dot{w} = -\frac{J_0}{w} - wK_0(x_0, w, s, R),$$
$$I_1 \dot{x}_0 + I_2 \dot{w} = -\frac{J_1}{w} - wK_1(x_0, w, s, R),$$

where

$$I_n = \int_{-\infty}^{\infty} z^n \tilde{U}'(z)^2 dz,$$
$$J_n = \int_{-\infty}^{\infty} z^n \tilde{U}'(z)\tilde{U}''(z)dz,$$
$$K_n(x_0, w, s, R) = \int_{-\infty}^{\infty} z^n s(wz + x_0)R[\tilde{U}(z)]\tilde{U}'(z)dz.$$

The integrals I_n and J_n are numbers, they only depend on the profile $\tilde{U}$. In the cases that we consider, the determinant of the system is nonzero and we get the following equations governing $\dot{x}_0$ and $\dot{w}$:

$$\dot{x}_0 = \frac{\alpha_1}{w} + \alpha_2 wK_0(x_0, w, s, R) + \alpha_3 wK_1(x_0, w, s, R),$$
$$\dot{w} = \frac{\alpha_4}{w} + \alpha_5 wK_0(x_0, w, s, R) + \alpha_6 wK_1(x_0, w, s, R),$$

where

$$\alpha_1 = \frac{I_1 J_1 - I_2 J_0}{I_0 I_2 - I_1^2},$$

$$\alpha_2 = \frac{I_2}{I_1^2 - I_0 I_2},$$

$$\alpha_3 = \frac{I_1}{I_0 I_2 - I_1^2},$$

$$\alpha_4 = \frac{I_1 J_0 - I_0 J_1}{I_0 I_2 - I_1^2},$$

$$\alpha_5 = \frac{I_1}{I_0 I_2 - I_1^2},$$

$$\alpha_6 = \frac{I_0}{I_1^2 - I_0 I_2}.$$

APPENDIX B: EXACT VALUES OF INTEGRALS PRESENT IN THE PAPER

For the bistable case,

$$I_0 = \int_{-\infty}^{\infty} \tilde{U}'(z)^2 dz = \frac{1}{6},$$

$$I_1 = \int_{-\infty}^{\infty} z\tilde{U}'(z)^2 dz = 0,$$

$$I_2 = \int_{-\infty}^{\infty} z^2\tilde{U}'(z)^2 dz = \frac{\pi^2 - 6}{18} \approx 0.21,$$

$$J_0 = \int_{-\infty}^{\infty} \tilde{U}'(z)\tilde{U}''(z) dz = 0,$$

$$J_1 = \int_{-\infty}^{\infty} z\tilde{U}'(z)\tilde{U}''(z) dz = -\frac{1}{12},$$

$$K_0(x_0, w, 1, R_b) = \int_{-\infty}^{\infty} R_b[\tilde{U}(z)]\tilde{U}'(z) dz = \frac{2a - 1}{12},$$

$$K_1(x_0, w, 1, R_b) = \int_{-\infty}^{\infty} z R_b[\tilde{U}(z)]\tilde{U}'(z) dz = \frac{1}{24},$$

and the constants in (9) read

$$\alpha_1 = 0, \quad \alpha_2 = -6,$$

$$\alpha_3 = 0, \quad \alpha_4 = \frac{1}{12 I_2} \approx 0.39,$$

$$\alpha_5 = 0, \quad \alpha_6 = -\frac{1}{I_2} \approx -4.7.$$

For the monostable case,

$$I_0 = \int_{-\infty}^{\infty} \tilde{U}'(z)^2 dz = \frac{1}{5},$$

$$I_1 = \int_{-\infty}^{\infty} z\tilde{U}'(z)^2 dz = \frac{\ln(1 + \sqrt{2})}{5} - \frac{1}{6}$$
$$\approx 0.0096,$$

$$I_2 = \int_{-\infty}^{\infty} z^2\tilde{U}'(z)^2 dz$$
$$= -\frac{1}{3} + \frac{\pi^2}{15} - \frac{\ln(1 + \sqrt{2})}{3}$$
$$+ \frac{[\ln(1 + \sqrt{2})]^2}{5}$$
$$\approx 0.19,$$

$$J_0 = \int_{-\infty}^{\infty} \tilde{U}'(z)\tilde{U}''(z) dz = 0,$$

$$J_1 = \int_{-\infty}^{\infty} z\tilde{U}'(z)\tilde{U}''(z) dz = -\frac{1}{10},$$

$$K_0(x_0, w, 1, R_m) = \int_{-\infty}^{\infty} R_m[\tilde{U}(z)]\tilde{U}'(z) dz = -\frac{1}{6},$$

$$K_1(x_0, w, 1, R_m) = \int_{-\infty}^{\infty} z R_m[\tilde{U}(z)]\tilde{U}'(z) dz$$
$$= \frac{7}{45} - \frac{\ln(1 + \sqrt{2})}{6} \approx 0.0087,$$

and the constants in (9) read

$$\alpha_1 = \frac{90 I_1}{85 - 12\pi^2} \approx -0.026, \quad \alpha_2 = \frac{900 I_2}{85 - 12\pi^2} \approx -5.0,$$

$$\alpha_3 = \frac{900 I_1}{12\pi^2 - 85} \approx 0.26, \quad \alpha_4 = \frac{18}{12\pi^2 - 85} \approx 0.54,$$

$$\alpha_5 = \frac{900 I_1}{12\pi^2 - 85} \approx 0.26, \quad \alpha_6 = \frac{180}{85 - 12\pi^2} \approx -5.4.$$

[1] Ya. B. Zeldovich and D. A. Frank-Kamenetsky, The theory of thermal propagation of flames, Zh. Fiz. Khim **12**, 100 (1938).

[2] A. Scott, *Nonlinear Science, Emergence and Dynamics of Coherent Structures*, 2nd ed. (Oxford University Press, Oxford, 2003).

[3] J. Xin, Front propagation in heterogeneous media, SIAM Rev. **42**, 161 (2000).

[4] K. R. Swanson, R. Rostomily, and E. C. Alvord, Jr., Predicting survival of patients with glioblastoma by combining a mathematical model and pre-operative MR imaging characteristics: A proof of principle, British J. Cancer **98**, 113 (2008).

[5] J. D. Murray, *Mathematical Biology I: An Introduction*, 3rd ed. (Springer, New York, 2002).

[6] R. Fisher, The wave of advance of advantageous genes, Ann. Eugenics **7**, 355 (1937).

[7] M. J. Ablowitz and A. Zeppetella, Explicit solutions of Fisher's equation for a special wave speed, Bull. Math. Biol. **41**, 835 (1979).

[8] J.-G. Caputo and B. Sarels, Reaction-diffusion front crossing a local defect, Phys. Rev. E **84**, 041108 (2011).

[9] J. H. P. Dawes and H. Susanto, Variational approximation and the use of collective coordinates, Phys. Rev. E **87**, 063202 (2013).

[10] J. Belmonte-Beitia, G. F. Calvo, and V. M. Perez-Garcia, Effective particle methods for Fisher-Kolmogorov equations: Theory and applications to brain tumor dynamics, Commun. Nonlinear Sci. Numer. Simulat. **19**, 3267 (2014).

[11] H. Mi, C. Petitjean, B. Dubray, P. Vera, and S. Ruan, Prediction of lung tumor evolution during radiotherapy in individual patients with PET, IEEE Trans. Med. Imaging **33**, 4 (2014).

[12] H. Berestycki, J. Bouhours, and G. Chapuisat, Front blocking and propagation in cylinders with varying cross section, *Calculus of Variations and Partial Differential Equations* (Springer, New York, 2016).

[13] J. Bouhours, Reaction diffusion equation in heterogeneous media: Persistance, propagation and effect of the geometry, *General Mathematics* (Université Pierre et Marie Curie, Paris, 2014).

[14] J. M. Roquejoffre, Convergence to travelling waves for solutions of a class of semilinear parabolic equations, J. Diff. Equ. **108**, 262 (1994).

[15] J. Garnier, T. Giletti, F. Hamel, and L. Roques, Inside dynamics of pulled and pushed fronts, J. Math. Pures Appl. **98**, 428 (2012).